nature reviews methods primers

https://doi.org/10.1038/s43586-023-00232-z

Primer

Check for updates

Terahertz time-domain spectroscopy

Martin Koch [1] ✉, Daniel M. Mittleman [2], Jan Ornik [1] & Enrique Castro-Camus [1]

Abstract

The terahertz band of the electromagnetic spectrum was the least explored region of the spectrum prior to the introduction of the technique known as time-domain spectroscopy (TDS) in the late 1980s. Since its introduction, terahertz TDS has enabled the study of a plethora of physical, chemical and biological phenomena; from excitons and Cooper pairs in solids to the hydration dynamics of biomolecules. Terahertz techniques can be used to non-destructively analyse samples from diverse fields, such as art conservation and industrial quality control, whereas terahertz imaging can act as a sensitive hydration probe in biological tissue and other materials. This article focuses on TDS, a unique hybrid between microwave and optical technologies. By measuring the time-dependent electric field waveform, rather than the intensity of the electromagnetic wave, one directly accesses the spectral amplitude and phase of the electric field. As a result, both the refractive index and absorption coefficient (or the complex dielectric function) of a sample can be measured simultaneously. The technique is based on the generation and detection of single-cycle pulses of radiation, enabling measurements with sub-picosecond time resolution. This Primer summarizes the basics of such systems and gives a few illustrative application examples.

Sections

[1]Department of Physics and Material Sciences Center, Philipps-Universität Marburg, Marburg, Germany.
[2]School of Engineering, Brown University, Providence, RI, USA. ✉e-mail: martin.koch@physik.uni-marburg.de

Introduction

The terahertz band of the electromagnetic spectrum spans from ~100 GHz (3 mm wavelength) to ~10 THz (30 μm) (see Fig. 1). Historically, this band was hard to access. For lower frequencies, powerful emission and sensitive detection can be achieved by using electronic circuits to produce oscillatory currents that generate electromagnetic radiation, or by using electromagnetic waves to drive a current that can be detected also with electronic circuits. This is the principle behind radio and television transmitters and receivers, microwave ovens and most telecommunication systems. Higher frequencies such as infrared, visible, ultraviolet, X-radiation and gamma-radiation can be produced by photon emission from relaxation between energy levels of quantum systems, such as molecules, atoms and atomic nuclei. High-frequency detection can also be achieved with quantum systems, such as semiconductors, that change their conductivity when excited by incoming radiation. The terahertz band falls between these two regimes of familiar technologies[1,2]. Yet, it is difficult to scale techniques from either of these realms into the terahertz range. Conventional electronic components cannot oscillate fast enough to produce significant amounts of power above ~300 GHz or detect high frequencies with reasonable sensitivity. This means it is challenging to use electronic technology for terahertz systems. Similarly, quantum systems present fundamental detection problems. Terahertz photons have small energies that are comparable with, or below, the thermal energy at room temperature. As a result, the signal is buried in an overwhelming noise background. The first, and now most widespread, technique that finally allowed the terahertz band to be accessed with extraordinary signal-to-noise performance is terahertz time-domain spectroscopy (TDS).

Prior to the development of terahertz TDS, the most common method for broadband access to this spectral range used a thermal blackbody — such as a glowing hot piece of metal — as the radiation source, for either direct spectroscopy or Fourier transform spectroscopy. Even when heated to well above 1,000 °C, these sources do not produce much radiation at frequencies below a few terahertz, making the measurements challenging. This situation began to change with the first demonstration of terahertz TDS[3,4], which relies on femtosecond laser pulses exciting a device that emits electromagnetic transients containing frequency components between 100 GHz and several terahertz. A receiver detects these transients and is gated by the same laser. The next key advance was the idea of using terahertz TDS to obtain two-dimensional images of objects[5]. In the simplest scheme, samples are raster-scanned through the focus and images are formed one pixel at a time. Much research has been devoted to exploring other imaging configurations and improving the performance of imaging systems[6].

A coarse schematic of a time-domain spectrometer, highlighting the main components, is shown in Fig. 2. Optical pulses emitted from a femtosecond laser excite the terahertz emitter. The emitted terahertz pulses then propagate in air, through a spectrometer which could contain a sample to be investigated. A second beam path for the optical pulses is introduced via a beam splitter. The pulses following this second path gate a terahertz detector, timed to arrive at the same moment when the terahertz pulse arrives. The terahertz pulse has duration of about 1 picosecond, typically about a factor of 10 longer than the optical pulse. As a result, the detector samples only a short portion of the terahertz waveform. In order to measure the full terahertz waveform, the arrival time of the optical gating pulse needs to be varied, relative to the arrival time of the terahertz pulse, using an optical delay line. The acquired signal, measured as a function of this time delay, can then be interpreted as being directly proportional to the time-domain electric field of the terahertz pulse; that is, the TDS nomenclature refers to the waveform being measured as a function of time. This time-domain measurement can be numerically processed via Fourier transform to obtain the spectral or frequency-domain information.

The earliest systems used photoconductive antennas as emitters and detectors. Subsequently, many types of terahertz emitters were demonstrated. Terahertz emission can be used to study a sample in the beam path or to investigate ultrafast physical processes in the emitter induced by optical excitation[7]. Several other schemes for coherent terahertz pulse detection — which is sensitive to the electric field, not merely the intensity — have also been demonstrated, with advantages and disadvantages for each. Antenna materials have been developed for compatibility with femtosecond fibre lasers, allowing the use of fibre-coupled antenna modules[8]. This enables free positioning and movement of terahertz antennas, providing enormous additional flexibility to TDS systems. Recently, robotic arm-based terahertz systems were demonstrated to investigate extended objects with arbitrary shapes[9,10]. Using such systems, tomographic information about the internal structure of samples can be acquired.

Terahertz TDS is now a widely used technique for studying the dielectric properties of samples in the lower terahertz range (0.1–3 THz). This encompasses various materials, including gases, liquids, liquid crystals and many types of solids, from semiconductors and superconductors to molecular crystals and more[11]. This Primer focuses on the most common techniques for generating and detecting terahertz pulses with femtosecond lasers, the basis of several commercial TDS systems. Given the rapid growth in the field, this Primer cannot review everything. Instead, a few example terahertz spectroscopic investigations and imaging applications are discussed to show the potential and versatility of the method.

Experimentation

Accessing the terahertz portion of the spectrum was historically difficult. This situation began to change with the introduction of terahertz TDS. The lack of broadly available techniques to access this band gave rise to the now obsolete terminology of the terahertz gap. A small but very active community has advanced the method, which cannot be considered a fully optical or fully electronic spectroscopic technique. In optics, the primary variable measured is the irradiance, or luminous intensity. In the optical range, electromagnetic waves have frequencies in the order of hundreds of terahertz, meaning the electric and magnetic fields oscillate too fast for any detector to directly resolve the time-dependent electric field waveform. Therefore, normally, the irradiance — the time average of the squared electric field amplitude — is measured. As a result, a typical measurement includes no information about the phase of the electric field. In the electronic region, corresponding to the radiofrequency and microwave bands with frequencies below ~100 GHz, antennas are used to couple electromagnetic waves to electrical circuits. This produces an oscillating current proportional to the electric field. A typical measurement accesses both the electric field amplitude and direction, preserving phase information. Terahertz TDS is a hybrid technique because it incorporates antenna structures into optically triggered semiconductor devices. Ultrafast laser pulses offer the possibility to produce and measure transients of electromagnetic radiation so short that they contain only one cycle of electromagnetic oscillation. This burst of radiation has spectral components spanning, typically, from 100 GHz to 3 THz (roughly 3–100 cm^{-1}), but bandwidths up to several tens of terahertz can be achieved. As the time-dependent waveform of the electric field

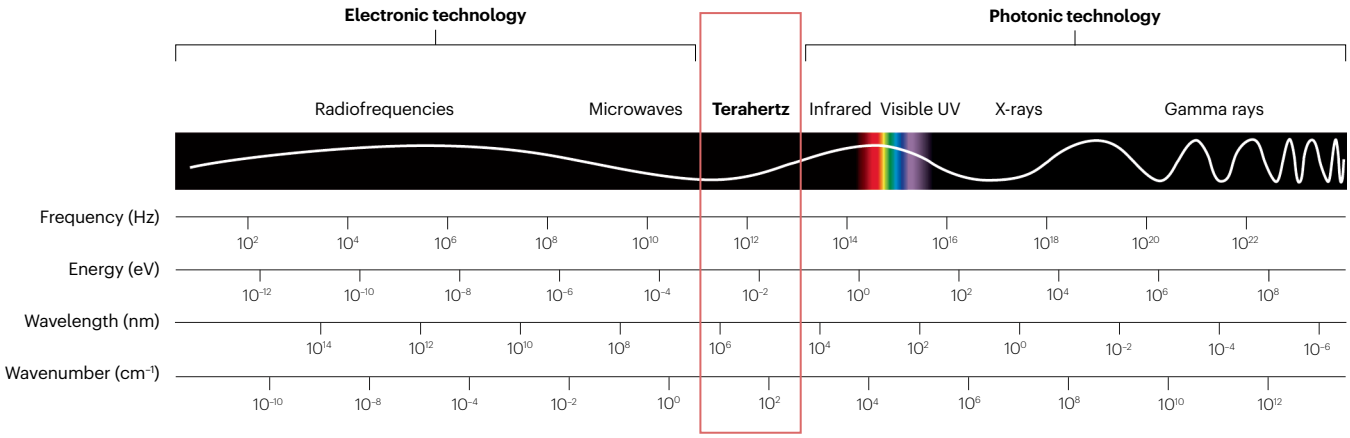

Fig. 1 | The electromagnetic spectrum highlighting the terahertz band. Names of the bands of each part of the spectrum (top), and various scales with different physical quantities that characterize the frequency of the radiation (bottom) as a reference.

$E(t)$ is directly measured, this technique allows direct determination of both the refractive index and the absorption coefficient of materials.

The typical terahertz TDS system has four basic building blocks, as shown in Fig. 2: an ultrafast laser producing a train of femtosecond pulses, a terahertz emitter, a terahertz detector and a delay line. The ultrafast source was traditionally a Ti:sapphire mode-locked laser centred near 800 nm, which is still the case for many home-built systems. However, Ti:sapphire lasers have been gradually replaced, particularly in commercial TDS systems, by more robust and economical rare-earth-doped fibre lasers with wavelengths centred between 1,000 nm and 1,600 nm. These ultrafast lasers provide pulses of near-infrared light with durations typically of 100 fs or less. In the TDS system, a beam splitter is used to separate this train of pulses into two beams. One is directed to a delay line, typically a pair of mirrors mounted on a motorized platform, to vary the path length and control the time taken to reach the emitter. The emitter converts the optical pulse into an electromagnetic transient, usually one or a few cycles of the electric field. Meanwhile, the second laser pulse is directed to the detector. The detector produces a signal proportional to the instantaneous electric field of the terahertz pulse, which occurs the instant it is gated by the second laser pulse. By moving the delay line and changing the arrival time of the terahertz transient relative to the second (gate) pulse, the electric field of the terahertz waveform can be mapped one point at a time. This point by point assembly of the full time-domain waveform is known as a sampling measurement. The two most common detection schemes are photoconductive sampling and electro-optic sampling. In both cases, signals are typically small and a lock-in amplifier is often used to isolate these signals from background noise. Several commercial systems are available based on fibre lasers, where both the emitter and the detector are fibre-coupled and the delay line is completely enclosed. Fibre coupling enables easy transportation and reconfiguration of the system and offers significant improvements in robustness and ease of use. An outline of the typical data acquisition process is given in Supplementary Box 1.

Mechanical delay lines, as shown in Fig. 2, are common. However, the high-mass components of the delay lines are inertial and cannot be moved arbitrarily fast. As a result, they only allow relatively slow sampling of the terahertz waveform. Typical commercial systems can scan a delay window of 100 ps at a rate of 50 Hz. In some cases, faster data acquisition is desired. Faster measurement methods that do not require heavy mechanical components have been developed. Asynchronous optical sampling[12,13] and electrically controlled optical sampling[14,15] use two lasers with slightly different pulse repetition rates. A related technique is optical scanning by cavity tuning[16], which uses only one laser.

The schematic drawing in Fig. 2 shows terahertz transmitters and receivers, between which a sample is placed. This path usually contains optical components suitable for terahertz frequencies (not shown in Fig. 2). For example, off-axis parabolic mirrors or lenses — typically made of a plastic such as polyethylene, TPX or Teflon — are often used. The frequency spectrum of broadband terahertz pulses covers at least one order of magnitude, often close to two. Owing to the diffraction limit, the high-frequency components within these pulses can be focused tighter than the low-frequency components, an effect that must be considered in terahertz imaging systems. The dimensions of the optical components are often only one or two orders of magnitude above the wavelength of the radiation, particularly for lower frequency components in the terahertz pulse. As a result, diffraction becomes important, and therefore these systems operate in a quasi-optics regime rather than the regime of conventional optics[17]. Ray-tracing programs, often used to design optical systems, do not always provide accurate results in these cases.

A terahertz TDS system can also be configured to record the measured signal in reflection. The emitter and the detector are placed at equal angles with respect to the normal to the sample surface. Parameters involved in transmission also play a role in reflection, but in a different manner, meaning signal analysis is performed differently. A reflection geometry is preferred for materials that are too reflective or lossy to permit transmission, such as highly conductive materials or polar liquids. For a sample with multiple layers, short pulses can be exploited to obtain information on the layer thickness by measuring the relative delay of the reflections from each interface[18]. Tomographic images can be obtained if the interfaces between layers are approximately parallel and the layers are sufficiently transparent and also thick enough so that sequential reflections do not overlap temporally.

Another important variation of the TDS technique is optical-pump terahertz-probe spectroscopy[19]. This approach uses an additional beam splitter to separate a fraction of the near-infrared laser pulse

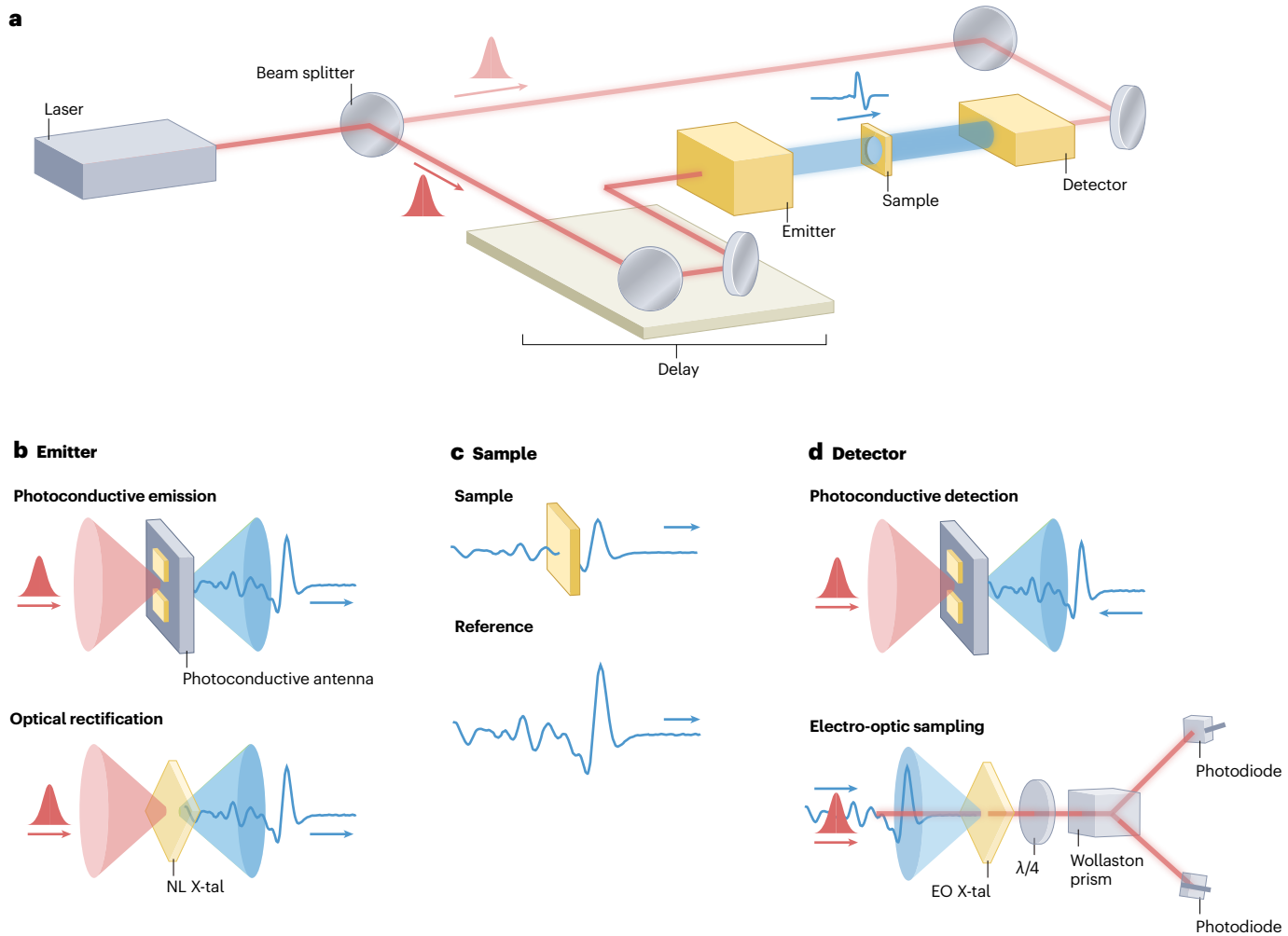

Fig. 2 | Simplified terahertz time-domain spectrometer. a, Three-dimensional representation of a terahertz time-domain spectrometer. **b**, Two main types of emitters. A photoconductive antenna — a piece of insulating semiconductor under bias through two contacts (gold) — emits radiation through the sudden separation of electrons and holes after ultrafast photoexcitation. Optical rectification occurs when an ultrafast pulse propagates through a material with non-zero second-order optical response (NL X-tal). **c**, Two waveforms: a reference in the absence of a sample; and one propagated through a sample, represented by a yellow slab. The amplitude of the sample waveform decreases with respect to the reference due to absorption, scattering and reflections at the sample interfaces. The waveform is delayed and changes shape due to the greater, frequency-dependent refractive index of the sample compared with the reference. **d**, The two most common detection methods. Using a photoconductive antenna, where an ultrafast laser pulse increases the conductivity — at the same time, a terahertz pulse arrives, producing a current between the electrodes proportional to the instantaneous electric field. When the two pulses are delayed with respect to the other, the current follows the time-dependent shape of the terahertz pulse. Electro-optic sampling, where an electro-optic material (EO X-tal) changes its birefringence proportionally to the instantaneous electric field of the terahertz transient. This birefringence modifies the polarization of the ultrafast pulse. A quarter-waveplate ($\lambda/4$) is used to convert the linearly polarized light into circularly polarized light, before a Wollaston prism separates the beam into a horizontally and vertically polarized beam. The instantaneous electric field of the terahertz transient causes a disbalance of the intensities between the two beams, which are detected by a pair of photodiodes. By delaying the two pulses it is possible to map out the waveform of the terahertz transient.

into a third beam. The extra beam, called the pump, excites the sample before the terahertz-probe pulse arrives, enabling the terahertz dielectric properties of a photo-excited sample to be measured. By varying the time delay between the optical-pump pulse and the terahertz-probe pulse, the temporal variation of these properties following optical excitation can be mapped out. With this technique it is possible to monitor the evolution of, for example, photo-induced conductivity in a sample, with picosecond resolution. This powerful tool has been used to reveal the ultrafast optoelectronic properties of many different materials[20–23]. The sample excitation wavelength can be chosen by using an optical parametric amplifier, a second harmonic-generation crystal or other non-linear optical processes when needed. A detailed description of the optical-pump terahertz-probe technique can be found elsewhere[24].

Terahertz generation

Photoconductive emitters. A photoconductive emitter, also known as an Auston switch, consists of a pair of metallic electrodes, which form an antenna with a gap, on a highly resistive semiconductor substrate.

Common substrate materials used for excitation at 800 nm include semi-insulating GaAs, low temperature-grown GaAs, ion-implanted GaAs or InP[25]. For excitation by fibre lasers, multilayer InGaAs heterostructures[26] and doped InGaAs layers are often used[27,28]. A large DC electric field, typically >1 kV cm^{-1}, is applied across the gap between the two metal electrodes. The high resistivity of the substrate means that only a small dark current is induced. If an ultrashort (<1 ps) laser pulse is used to generate free charges (photo-carriers) by optical absorption in the gap between the electrodes, these charges will accelerate in the applied DC field. This rapidly varying current J leads to the formation of a time-dependent dipole, which gives rise to a burst of electromagnetic radiation[29], E_{THz}, in accordance with Maxwell's equations that state accelerating charges produce radiation according to:

$$E_{\mathrm{THz}} \propto \frac{\partial J}{\partial t} = \frac{\partial}{\partial t}(nev) \tag{1}$$

where n is the charge carrier density, e is the electron charge and v is the charge velocity. As $n(t)$ and $v(t)$ both vary on the timescale of the laser pulse, this derivative produces a pulse of radiation with a duration $\lesssim$1 ps and containing a broad distribution of frequencies around 1 THz. Most of the energy in this burst of radiation propagates into the semiconductor substrate[30] and can be efficiently coupled out of the back side of the semiconductor wafer into free space using a substrate lens[4].

Optical rectification. Optical rectification can occur in materials with non-zero bulk second-order dielectric susceptibility[31,32]. When a monochromatic wave of frequency ω, amplitude E_0 and electric field $E = E_0\cos(\omega t)$ travels through the material, a second-order dielectric polarization is generated, $P^{(2)} = \chi^{(2)}E_0^2\cos^2(\omega t)$, where $\chi^{(2)}$ is the second-order susceptibility of the material. This can be rewritten as $P^{(2)} = \chi^{(2)}E_0^2/2 - \chi^{(2)}E_0^2\cos(2\omega t)/2$. The first term, a zero-frequency polarization $P_0 = \chi^{(2)}E_0^2/2$, is of interest here. If an ultrashort laser pulse with a Gaussian temporal profile is used instead of a monochromatic wave, this zero-frequency polarization term can be rewritten as $P_0 = \chi^{(2)}E_0^2e^{-(t/\tau)^2}/2$, where τ is proportional to the duration of the pulse. This polarization, which changes in time, produces an electromagnetic pulse $E_{\mathrm{THz}} \propto \mathrm{d}^2P/\mathrm{d}t^2$ co-propagating with the Gaussian optical pulse. Unlike the photoconductive method, this is not purely a surface effect; efficient production of radiation using optical rectification requires an extended propagation range inside the non-linear medium. This implies that phase matching is needed to ensure the velocities of the incident optical radiation and the produced terahertz radiation are sufficiently similar. If not, the two radiation fields will become increasingly out of phase as they propagate. A thinner crystal offers improved phase matching and broader terahertz bandwidth, but lower emitted terahertz power. Phase matching considerations add complexity to the analysis but offer the advantage that this method can be used to produce terahertz pulses with much larger bandwidth than those produced by photoconductive antennas[33,34].

Terahertz detection

Photoconductive receivers. A photoconductive receiver is similar to a photoconductive emitter. It consists of a pair of metallic contacts with a gap between them, deposited on a semiconducting material. This is typically low temperature-grown GaAs — appropriate for gating at 800 nm — or a heterostructure of InGaAs layers, for gating with wavelengths above 1,000 nm. To use photoconductive detectors for time-domain electric field measurements, the carrier lifetime in the photoconductive material should be as short as possible. A short carrier lifetime is not a requirement for photoconductive emitters because the current transient is dominated by injection and acceleration of mobile carriers, rather than removal. An ultrashort laser pulse synchronized with terahertz transients is focused on the gap between the two contacts. The laser pulse is absorbed, rapidly changing the conductivity of the semiconductor due to photocarrier generation in the gap region. These charge carriers can be accelerated by the electric field of the incoming terahertz pulse to produce a measurable current between the two contacts:

$$I(t) = \frac{\mu e P_{\mathrm{G}} T_{12} \lambda}{hcW} \int_{-\infty}^{+\infty} E_{\mathrm{THz}}(t)\Phi(t-\tau)\mathrm{d}t \tag{2}$$

where τ is the relative delay between the terahertz and the optical pulse; μ is the mobility in the semiconductor; e is the electron charge; P_{G} is the optical power incident on the receiver; T_{12} is the Fresnel transmission coefficient; λ is the central wavelength of the laser; h is Planck's constant; c is the speed of light; W is the laser beam width; and $\Phi(t) \propto H(t)e^{-t/\tau_c}$ where H is a step function and τ_c is the carrier lifetime[35]. When the carrier lifetime in the material is short, the current only lasts for a brief time, typically a few hundred femtoseconds. In this case, $\Phi(t)$ can be approximated by a Dirac delta function. The current is then proportional to the instantaneous value of the terahertz electric field when the ultrafast pulse was absorbed[29]. By varying the delay between the laser pulse and the terahertz pulse, the terahertz electric field can be determined step by step in a sampling measurement.

Electro-optic sampling. Electro-optic sampling relies on the Pockels effect, a non-linear process where a linear, near-instantaneous change in the refractive index of a crystalline material is induced by the terahertz electric field. As a result, a birefringence is induced in the crystal. Propagating an ultrashort optical pulse collinearly with the terahertz pulse enables the birefringence to be characterized, by measuring the polarization state of the optical pulse. Typically, a Wollaston prism and a pair of balanced photodiodes are used to measure the polarization change. A $\lambda/4$ waveplate converts the linearly polarized incident wave into circular polarization, balancing the photodiodes in the absence of an applied terahertz electric field for sensitive differential measurement. As the laser pulse is much shorter than the terahertz pulse, the laser pulse's polarization change acts as a direct probe of one temporal point in the terahertz electric field waveform. Varying the delay of the laser pulse with respect to the terahertz pulse, the temporal profile of the terahertz electric field can be reconstructed step by step. The most widely used crystal for terahertz electro-optic sampling is ZnTe, as it offers excellent phase matching between an 800 nm optical pulse and a broadband terahertz pulse. Other materials, such as GaP and GaSe, have also been used. A disadvantage of this approach is that it is not easily implemented in a fibre-coupled package, which does not allow the terahertz and optical pulses to co-propagate through the non-linear crystal. The presence of lattice vibrations, phonons, in electro-optic crystals can lead to limitations on the usable bandwidth, both in the emission and the detection processes.

Sample preparation

In the basic system set-up depicted in Fig. 2, the sample is measured in a transmission geometry. The measured signal is determined by absorption as the pulse propagates, losses by Fresnel reflection as the pulse enters and leaves the sample, scattering produced by sample

inhomogeneities, retardation caused by the material's refractive index and multiple internal reflections within the sample. Transmission measurements are ideal to study samples with low or moderate losses from absorption or scattering because highly reflective or lossy samples allow no measurable signal to be detected. Examples include glasses, lightly doped semiconductors, polymers, gases, non-polar liquids or thin hydrated samples. As a rule of thumb, the sample should ideally have flat and parallel faces to avoid deviation of the terahertz beam path. It should be thick compared with the terahertz pulse duration multiplied by the speed of light, but not so thick as to produce optical aberrations that alter the alignment[36]. In other words, the sample should be thin compared with the confocal parameter of the terahertz beam. These issues do not arise if the terahertz beam is collimated.

The cross-sectional area of the sample surface should be large compared with the terahertz beam cross-section, which is typically on the order of 1 mm for a focused beam. Rigid materials can often be cut to comply with these geometrical characteristics. However, when the samples are gases or liquids, they must be contained in a cuvette or gas cell with parallel windows of well-characterized, terahertz-transparent materials that also comply with the geometrical constraints. Typical window materials are low-loss polymers, z-cut quartz or high-resistivity silicon.

Depending on the experimental aims, it is often desirable to maintain the terahertz radiation path in an environment without water vapour. Typically, all components between the emitter and the detector are enclosed in a chamber that can be purged with dry air or nitrogen, or where a vacuum pump can remove the air completely. This eliminates absorption caused by rotational modes of water molecules in the gas phase, which otherwise superimpose on the measured spectra but are not associated with the sample. However, purging is not always possible. Biological or valuable samples, such as artwork, cannot always be subjected to purged conditions. In such cases, the contribution of water vapour can be numerically removed from the signals. Sometimes, spectrally narrow absorption features will not affect the desired information in the signal. In addition, some spectrometers can incorporate a cryostat or oven to control the temperature of the material under study, or a flow cell for liquid samples. In the transmission geometry, the sample is usually mounted at normal incidence with respect to the propagation direction of the terahertz radiation. This prevents signal losses caused by lateral shift of the terahertz beam, which occurs due to refraction in the sample. Sample holders should have clear apertures that are larger than the terahertz beam spot, usually of at least several millimetres. This avoids artefacts in the waveforms caused by diffraction or shadowing of the signal due to the mount. If the sample is too small, and a small aperture is needed, this must be considered by acquiring a reference waveform with the aperture mounted in the exact same position, but in the absence of sample. The aperture can sometimes behave as a waveguide, and therefore the attenuation of the terahertz signal may contain contributions from the sample absorption and the impedance mismatch between free space and the aperture. Both contributions can change in the reference measurement.

Safety and ethical considerations

The number of biological and medical applications for terahertz science is increasing. Ethical considerations for any study involving animal or human subjects are set by the standard practices in those fields, relating to handling of animals, informed consent and approval of studies by relevant committees. In this context, it is worth noting that terahertz radiation is non-ionizing. Also, typical average powers available in terahertz TDS spectrometers are in the microwatt range, which is lower than the thermal terahertz radiation emitted by a room-temperature blackbody source. The dominant interaction between terahertz radiation and biological tissue is absorption of the radiation by liquid water. This can lead to heating if the power is sufficiently high. However, at microwatt power levels, heating effects are completely negligible in macroscopic samples. As a result, there is no reason to believe that exposure to radiation produced by a terahertz TDS spectrometer could cause any biological effect[37,38]. The number of studies on humans is still relatively limited, but no evidence of any effect from terahertz radiation within the TDS scheme has been reported. However, some time-domain spectrometers are based on amplified laser systems at kilohertz pulse repetition rates, which are designed to produce much higher peak electric fields, although with lower average power[39]. These large-peak fields are high enough to induce non-linear effects in materials, and could therefore cause damage in biological systems via non-thermal mechanisms[40].

Results

A typical time-domain waveform recorded with a transmission terahertz TDS set-up is shown in Fig. 3a. The recorded signal prior to the main terahertz pulse is expected to be zero because at these delay values the generated terahertz radiation has not yet reached the detector. The recorded signal reflects the noise level of the measurement system, including DC offset that may arise from bias offsets in electrical amplifiers. As a result, a common first step in signal processing is to offset-correct the original measured signal by subtracting the average value of the signal at early time delays. In Fig. 3a, this procedure has been implemented by averaging the first 5 ps of the waveform, which is earlier than the main terahertz pulse located at approximately 10 ps. In contrast to the signal preceding the terahertz pulse, the part of the waveform following the terahertz pulse does not need to be zero. This signal corresponds to the emitted terahertz radiation and its interaction with objects in the beam path between the emitter and the detector, for example terahertz lenses, a sample or the surrounding air. These interactions can distort the initially few-cycle transient, resulting in extended signals that can last for many picoseconds after the main pulse. This part of the waveform carries valuable information about these interactions. As an illustration, the waveform shown in Fig. 3a was recorded in ambient conditions of humidity and temperature. The signal oscillations after the terahertz pulse reflect the interaction of the terahertz radiation with water vapour in the beam path.

Correcting a DC offset is only the first step in processing raw data. For example, it is often desirable to window the measured signals. In effect, windowing of the terahertz waveform is unavoidable, as every recorded waveform samples a finite time window. This corresponds to an infinite-duration signal multiplied by a rectangular window function of duration equal to the measurement window. A rectangular window can introduce undesirable artefacts in the Fourier domain, particularly if the signal is not zero at the window edges. It is thus often useful to introduce a window function to ensure that the signal goes smoothly to zero at both ends. A Hann window is plotted in Fig. 3a, scaled with the maximum value of the offset-corrected waveform. The signal is windowed by multiplication with the non-scaled window function to guarantee a smooth and continuous reduction of the signal values to zero at the edge of the window. Windowing can also reduce spectral leakage, and the selection of the window function can influence the dynamic range of the measurement, as well as properties of the observed absorption features in the frequency domain[41].

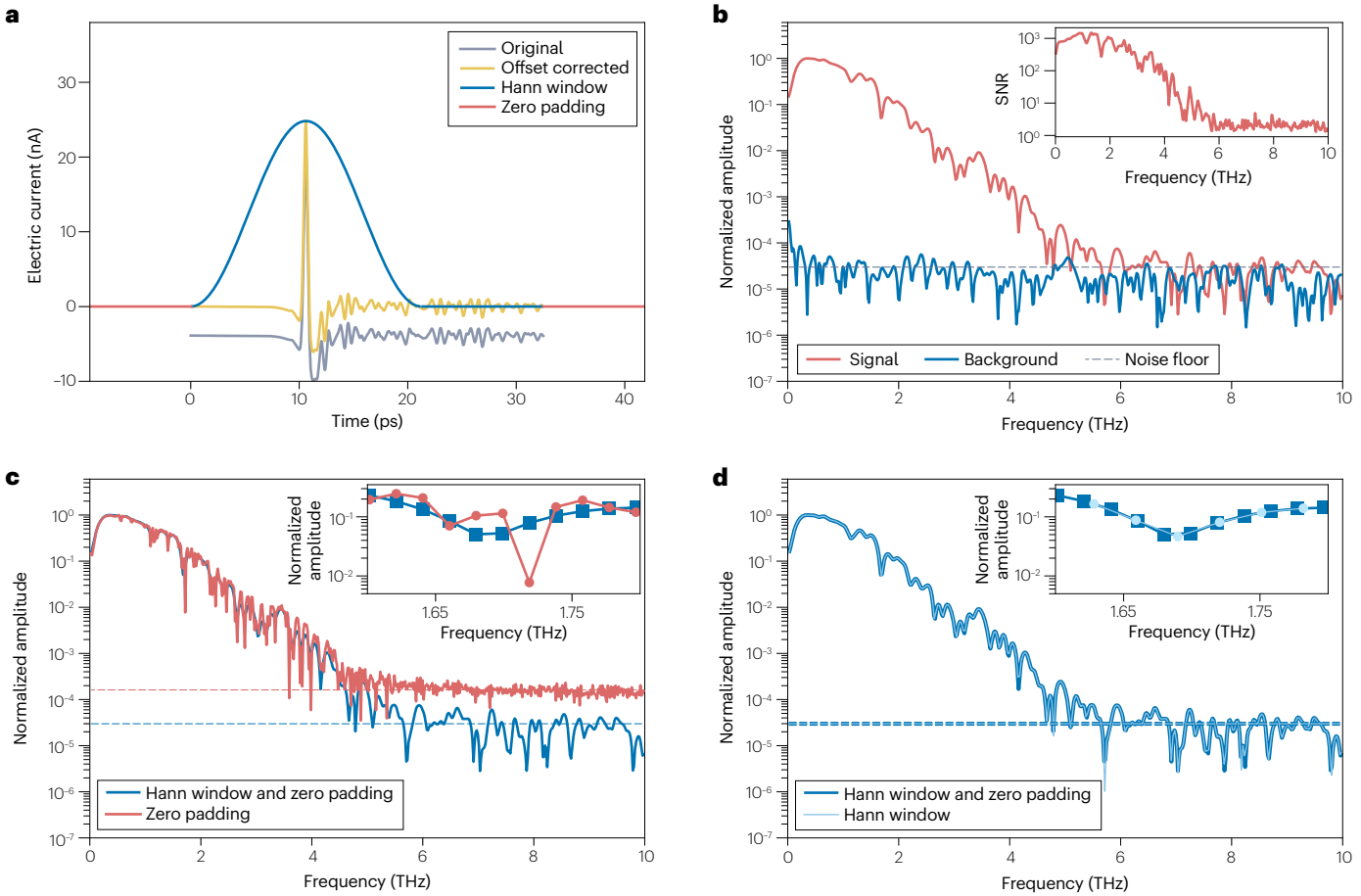

Fig. 3 | Terahertz time-domain signal processing I: basic processing steps. **a**, Terahertz waveform recorded with a terahertz time-domain spectroscopy (TDS) system based on photoconductive antennas and a femtosecond laser. **b**, Normalized amplitude obtained by performing fast Fourier transform of the offset-corrected, windowed and zero-padded waveform. Dotted line indicates the noise floor estimated as the root mean square value of the signal at frequencies above 6 THz. Background measurement corresponds to the measurement performed while blocking the terahertz beam with a metal object. Inset: signal-to-noise ratio (SNR) calculated from ten repeated measurements. Measurements were performed at ambient humidity and temperature without a sample in the terahertz beam path. **c**,**d**, Effect of windowing and zero padding on the frequency-domain data. Dark blue curves correspond to the spectrum shown in panel **b**; the offset-corrected, windowed and zero-padded signal. Dashed lines indicate the noise floor. Insets: narrow part of the spectrum centred around 1.7 THz, where a spectral feature can be observed. This feature is due to interaction of the terahertz radiation with water vapour in the ambient air. **c**, Effect of the Hann window on the obtained spectrum. Applying the Hann window to the offset-corrected signal before zero padding (dark blue curve) results in a lower noise floor compared with only zero padding of the offset-corrected signal (red curve). Inset: effect of windowing on the shape of the spectral feature — the apparent frequency resolution of the two signals does not differ. **d**, Effect of zero padding the signal after applying the Hann window on the obtained spectrum. Zero padding does not substantially alter the overall spectrum; however, it results in an apparently greater frequency resolution (inset).

After offset correction and windowing, a discrete Fourier transformation algorithm transforms the signal into the frequency domain. In a Fourier-transformed signal, the spacing between adjacent points in the frequency domain is given by the inverse of the total duration of the temporal signal. This sets the spectral resolution of a measurement made with a time-domain spectrometer. For instance, the waveform in Fig. 3 extends over a temporal window of about 33 ps, giving a spectral resolution of 30 GHz. An additional step, known as zero padding, is often used at this stage. Zero padding is an extension of the measured signal by adding zeros before and/or after the recorded signal to increase the total length of the signal in the time domain. This can be useful when signals of different lengths are analysed and compared. Converting a zero-padded signal into the frequency domain via a Fourier transformation results in an apparently higher frequency resolution because the temporal window is longer. However, this does not improve the actual spectral resolution of the measurement. The apparent improvement can be understood as an interpolation of the data in the frequency domain[42]. An example of how windowing and zero padding can affect the frequency-domain signal is depicted in Fig. 3c,d. Without applying an appropriate window function, zero padding can lead to discontinuity in the signal and artefacts in the frequency-domain data.

The transformed, offset-corrected, windowed and zero-padded time-domain signal is plotted in Fig. 3b on a semi-log scale in terms of the normalized electric field amplitude with respect to the frequency. In this example, the greatest signal amplitude can be observed between 0.3 and 0.6 THz. This is followed at higher frequencies by a

very rapid decrease of the signal amplitude. At a certain point, this rapid decrease exhibits a sudden change in slope, where the signal flattens and becomes nearly constant. This is the frequency at which the signal has reached the noise floor of the measurement. In the example in Fig. 3b, at frequencies exceeding 5 THz, only noise is detected. This can be verified by blocking the terahertz beam path with an opaque object and recording a background signal (Fig. 3b, blue curve). The usable range is the frequency range where the signal exceeds the noise floor, typically from few hundred gigahertz up to several terahertz. A commonly reported property of a terahertz TDS system is its dynamic range, defined as the ratio between the signal and noise level, which describes the maximum detectable signal change[43]. Often, only the peak dynamic range is reported, although this quantity is frequency-dependent. In the signal shown in Fig. 3b, the peak dynamic range exceeds four orders of magnitude in terms of electric field amplitude. This corresponds to eight orders of magnitude, or 80 dB, in the intensity. As the noise floor is roughly frequency-independent, the dynamic range can be estimated from a single measurement. Another important property is the signal-to-noise ratio (SNR), which is related to the smallest detectable change in the measured signal. The inset in Fig. 3b shows the SNR of the system, which was calculated from a set of repeated measurements as the average amplitude divided by the standard deviation of the amplitude. The SNR is frequency-dependent, with a shape resembling the signal amplitude.

Another important example of time-domain windowing can arise in the situation where the terahertz beam encounters a flat solid slab of material. This could be a planar sample under study, or the windows of a cell containing a fluid sample. In such situations, the time-domain waveform may appear to contain one or more copies of the initial single-cycle transient. These can arise from multiple reflections between the two flat parallel surfaces. An example is illustrated in Fig. 4. The sample waveform in Fig. 4a (yellow curve) exhibits two smaller replicas of the initial transient, at delays of roughly 34.5 ps and 46.4 ps, following the main transient at 22.6 ps. The delay between the main peak and the first replica, indicated by Δt in Fig. 4a, is the two-way travel time for radiation between the two reflecting surfaces. A Fourier transform of the waveform exhibits a modulation superimposed on the initial broadband pulse spectrum, with periodicity $\Delta\upsilon = 1/\Delta t$ (see Fig. 4b). These features can appear to indicate the presence of absorption resonances in the material but instead are a manifestation of the Fabry–Perot effect. In many cases, it is desirable to eliminate them from subsequent spectral analysis. One appropriate method for accomplishing this is to use a windowing procedure. By defining a window function that zeros out the replicas in the time-domain waveform, the periodic modulation of the resulting Fourier spectrum is largely suppressed (Fig. 4b, blue curve). These time-domain features may also be exploited, rather than eliminated, as discussed elsewhere[44–46].

A typical experiment consists of at least two time-domain waveform measurements: one with the sample present in the beam path and a second, called the reference, with the sample removed. Comparing these two measured signals enables spectroscopic information to be extracted. Typically, this comparison is implemented in the frequency domain to extract a sample's frequency-dependent dielectric parameters over the spectral range covered by the terahertz pulse. The propagation of an electromagnetic wave from the transmitter to the receiver is described by a frequency-dependent transfer function:

$$E_{\mathrm{R}}(\omega) = E_{\mathrm{T}}(\omega)H(\omega) \tag{3}$$

where $E_{\mathrm{T}}(\omega)$ is the electric field produced by the transmitter, $E_{\mathrm{R}}(\omega)$ is the electric field arriving at the detector and $H(\omega)$ is a linear transfer function that incorporates all intervening propagation effects. This expression can be rewritten for the two situations, sample and reference:

$$E_{\mathrm{Ref}}(\omega) = E_{\mathrm{T}}(\omega)H_0(\omega)$$

$$E_{\mathrm{Samp}}(\omega) = E_{\mathrm{T}}(\omega)H_{\mathrm{S}}(\omega) \tag{4}$$

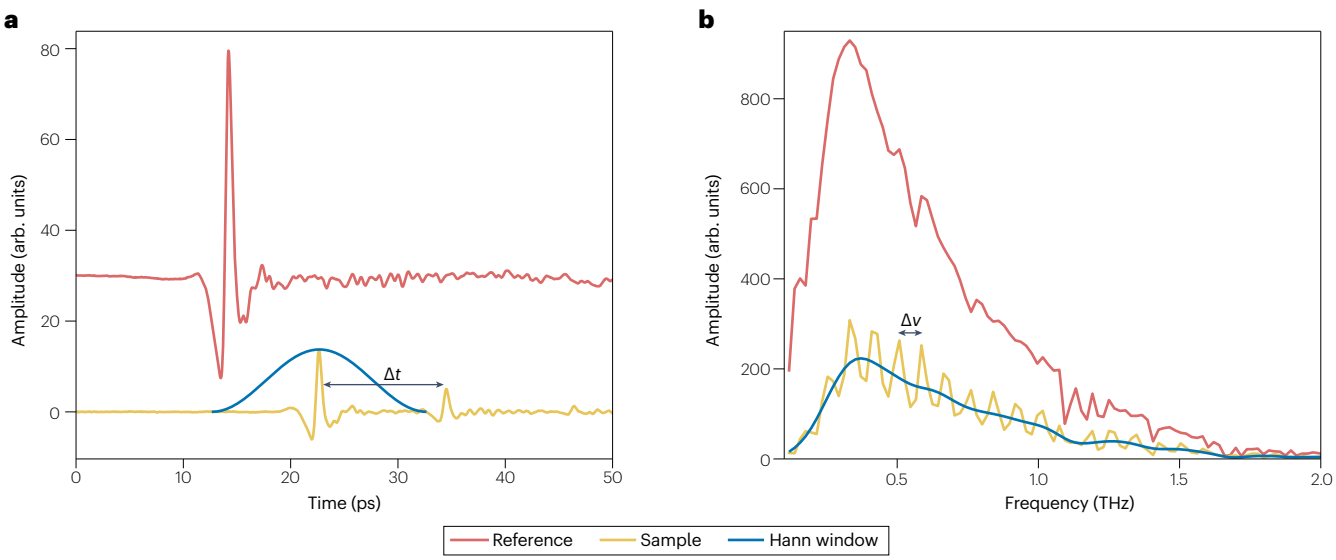

Fig. 4 | Terahertz time-domain signal processing II: eliminating multiple reflections. a,**b**, Terahertz processing in the time domain (panel **a**) and the resulting changes in the frequency domain (panel **b**). Blue line in panel **b** corresponds to the windowed time-domain data that exclude the Fabry–Perot contribution by eliminating the two replica pulses. Δt, temporal separation between the initial transmitted pulse and the first replica pulse; $\Delta\nu$, frequency separation between the oscillations caused by the presence of replica pulses.

where $H_S(\omega)$ and $H_0(\omega)$ describe the transfer functions connecting the transmitter to the detector when a sample is present in the beam path and when it is not, respectively. By taking the ratio of these two measured electric fields, $E_{Samp}(\omega)/E_{Ref}(\omega)$, the transmitted field $E_T(\omega)$ (which cannot be measured) is eliminated from the analysis. An analytical expression is needed for the two transfer functions, which depends on the sample material properties, such as the complex dielectric function $\varepsilon(\omega)$.

As an illustration, a sample consisting of a solid homogeneous slab of material with thickness L and smooth parallel surfaces oriented perpendicular to the propagation direction is considered. In the analytic expressions for $H_0(\omega)$ and $H_S(\omega)$, the effects of propagation outside length L can be ignored as they are identical for both measurements and cancel out in the ratio procedure. Thus, the reference measurement transfer function $H_0(\omega)$ is the electromagnetic propagator for a length L of empty space:

$$H_0(\omega) = e^{-i\omega L/c} \tag{5}$$

For the sample measurement, ignoring multiple reflections in the slab — such as those in the sample waveform in Fig. 4a — the transfer function $H_S(\omega)$ is:

$$H_S(\omega) = T_{12}(\omega)e^{-\alpha(\omega)L/2}e^{-\mathrm{in}(\omega)\omega L/c}T_{21}(\omega) \tag{6}$$

where $T_{12}(\omega)$ and $T_{21}(\omega)$ are the Fresnel transmission coefficients for the front and back surfaces, assumed to be real numbers — a good approximation for a weakly absorbing medium; $\alpha(\omega)$ is the absorption coefficient of the material; and $n(\omega)$ is its refractive index. The ratio of the two experimentally measured quantities:

$$\angle\left(\frac{E_{Samp}(\omega)}{E_{Ref}(\omega)}\right) = e^{-i[n(\omega)-1]\omega L/c}$$

$$\left|\frac{E_{Samp}(\omega)}{E_{Ref}(\omega)}\right| = T_{12}(\omega)T_{21}(\omega)e^{-\alpha(\omega)L/2} \tag{7}$$

can be used to obtain the material properties. This description of the simplest possible spectroscopic measurement can be adjusted for various different measurement configurations or situations, including sample measurements in a reflection configuration, rather than transmission[47]. In reflection measurements, a key experimental challenge is to acquire a reference measurement where the sample is replaced by a flat metal reflector located at the same position. Typically, the change in phase due to reflection is small compared with, for example, the phase acquired by transmitting through a slab — even a small phase shift from a positioning error of the reference reflector can lead to notable errors in the extracted material parameters[48]. An alternative approach is to use a relatively thick transparent window as a superstrate and simultaneously measure reflection from the air–window interface and the time-delayed window–sample interface in the same waveform. If the dielectric properties of the window material are well known, the first reflected terahertz pulse can be used as a reference for determining the material properties that give rise to the second pulse[49,50]. This method is particularly useful in measurements of liquids[51], where the second window–sample interface can be confirmed as spatially homogeneous. Reflection measurements are particularly advantageous if high absorption in the sample rapidly attenuates any transmitted radiation to below the noise floor of the measurement[52]. In addition to transmission and reflection, other configurations have been implemented, including attenuated total internal reflection[53,54], ellipsometry[55], microfluidic platforms[56] and waveguide-based approaches[57].

Glossary

Birefringence
Electromagnetic radiation propagates in materials at a speed that is usually lower than the speed of light in vacuum, measured by the refractive index of the material. Some materials show not only one but two different speeds that depend on the polarization of the light. These materials are said to be birefringent. Birefringence is the difference of the two refractive indices.

Electromagnetic transients
Short pulses of electromagnetic radiation that contain only one or just very few cycles of oscillation.

Fabry–Perot effect
The interference effect of multiple reflections of a wave that appears in a layer of material.

Fourier transform
A mathematical operation that acts on a function f of a variable, such as time, and that finds its components F as a function of another variable, in this case the frequency. It is an operation that calculates how much of each frequency (the amplitude of the spectrum) is present in the original function f, and the relative delay of each frequency (the phase spectrum).

Windowing
An operation applied on a function f of a variable x that multiplies it by another function W also of the variable x. Usually the window function is 1 at certain value of x, typically corresponding to the maximum of f. The window either tends to zero at the ends of the domain or goes to zero within a smaller interval and remains at zero from those points onwards.

Applications

A detailed review of all applications is beyond the scope of this Primer; however, this section gives an overview of some areas where terahertz TDS has become a valuable tool. The first area is spectroscopy of materials. Terahertz TDS provides access to a range of the spectrum that is otherwise challenging to measure using other spectroscopic techniques. The rotational modes of polar molecules in the gas phase, which occur in the terahertz range, have been studied for many years[58,59] due, in part, to their relevance in astrophysics. Terahertz TDS has been used to demonstrate that many fundamental aspects of condensed-phase materials can be understood by measuring their dielectric properties in the terahertz range. For instance, although localized bond vibrations typically oscillate at much higher frequencies, the modes associated with collective molecular vibrations often fall in the terahertz range. These modes are associated with long-range crystalline order in molecular solids and typically possess both intermolecular and intramolecular character[60]. These modes are often uniquely associated with a specific crystal structure and molecular conformation. As a result, they can be regarded as a fingerprint spectrum for a given solid, analogous to fingerprint spectra of individual bonds in the infrared regime used to identify materials. Such modes have been studied extensively for many molecular crystals[61–64] and can be assigned using advanced density functional theory simulations to accurately account for weaker dispersion forces that define the potential energy surfaces[65,66]. These measurements give valuable

insights into the connection between terahertz vibrational modes and macroscopic properties, such as thermodynamic quantities[67]. For example, terahertz vibrational modes of molecular solids can play a pivotal role in phase transitions[68]; macroscopic properties, such as thermoelasticity[69]; or conductivity in disordered materials[70].

Free charge carriers in solids give rise to conductivity and enable electronic device operation. To discuss the spectroscopic properties of mobile charges, a classical model such as Drude theory is used as a starting point. Drude theory describes a resonant response in the limit where the resonance frequency is zero. This description often works well to describe mobile charges in the terahertz range and is widely used to understand charge transport in semiconductors[71,72]. Such a simple description is inadequate for describing more subtle effects, for example correlations between electrons and holes, which cause excitonic effects that can be particularly pronounced in nanostructured materials, such as quantum wells[73,74] or quantum dots[75].

The strong absorption of liquid water in the terahertz range means that terahertz spectroscopy offers unique possibilities for probing aqueous systems. Despite decades of study, questions remain about the dynamics of water molecules in the liquid phase. Understanding liquid water is relevant to many biological processes, as the dynamics of solvated molecules can be strongly influenced by coupling to the dense spectrum of vibrational modes of the solvent[76]. Terahertz spectroscopy provides important contributions[77,78], as the most relevant modes often fall in the terahertz regime. New techniques, such as polarization varying anisotropy terahertz microscopy, offer exciting insights into protein intramolecular vibrations[79].

A key application of terahertz technology is in imaging. For terahertz TDS, it is possible to obtain a full time-domain waveform and a complete broadband terahertz spectrum at each pixel of an image. This is accomplished by raster scanning the sample through the focus of the terahertz beam. Although this process is too slow for many applications, it has the advantage of providing a full multispectral data set for sample characterization. When forming an image, any spectroscopic features can be exploited as a contrast mechanism to investigate sample properties. For instance, a measurement of polarization-resolved Drude conductivity can highlight inhomogeneities in the doping of semiconductor wafers[80]. Vibrational features can be used for material identification in images and for chemical mapping[81]. In heterogeneous biological systems, terahertz measurements can probe hydration in corneal tissue[82] or assess the progress of diabetic foot disease[83].

Terahertz spectroscopy can be used in a diverse range of experiments. For example, it can be used to study liquid crystals, which must be contained in a cuvette for the measurement. Multiple reflections may occur, within the cuvette windows and between the front and rear windows. All reflections can lead to time-delayed signals in the terahertz waveform, confounding extraction of material parameters. Fortunately, obtaining accurate information about the terahertz dielectric properties of the cuvette materials makes it possible to deconvolve these effects[84] and derive accurate anisotropic material properties. Figure 5 illustrates an example for the liquid crystal PCH5, showing the significant birefringence and diattenuation across the terahertz spectral range[85].

Another example is a structure with many alternating layers of two transparent materials, each with a thickness on the order of the terahertz wavelength. In such a system, multiple reflections are induced intentionally to form, for example, a band of frequencies in which the structure exhibits high reflectivity, such as a Bragg mirror. Figure 6 shows the measured and predicted reflection spectra of this type of structure, where the alternating layers are composed of polypropylene and polyvinylidene fluoride, two polymers with high terahertz transparency. These multilayer structures act as efficient dielectric mirrors near 0.2 THz, for both incident polarizations and over a wide range of incident angles[86].

Medical applications of terahertz radiation have attracted intensive investigation. As noted above, time-domain systems typically operate in the sub-milliwatt range. The non-ionizing character of this radiation makes it inherently safe for in vivo spectroscopy and imaging. The strong attenuation of terahertz waves by water means it cannot replace X-rays for imaging internal structures, but other aspects have been explored. For example, terahertz radiation can be used to distinguish healthy and cancerous tissues[87], although the mechanism behind this contrast is still debated. The presence of water can also be an advantage when water-content variations act as a marker for a medical condition. This occurs in diabetic foot syndrome, a consequence of diabetes mellitus. Many patients with diabetes develop this condition, as elevated blood glucose levels deteriorate the vasculature and nerves in the lower limbs. The combination of

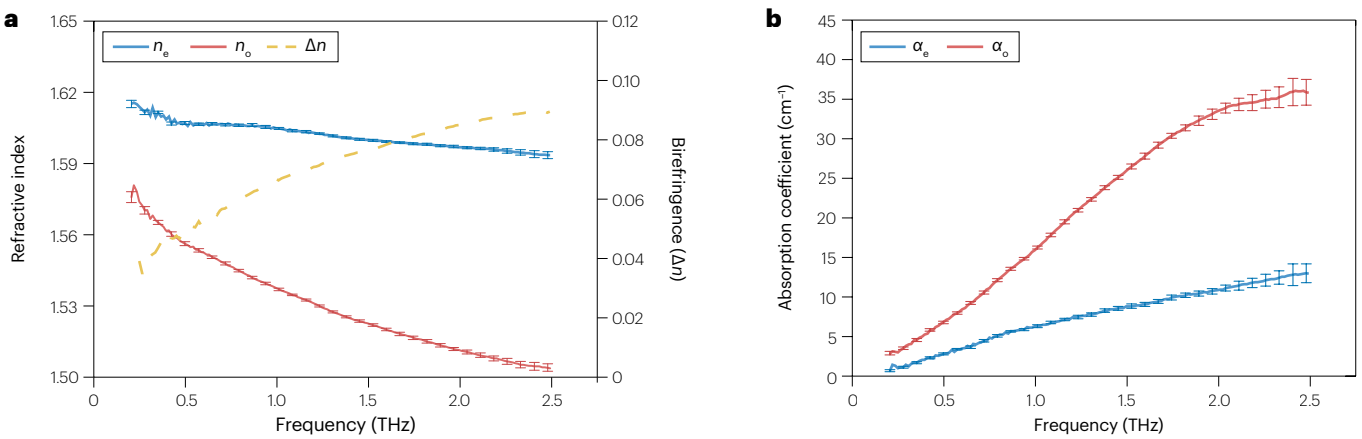

Fig. 5 | Terahertz birefringence of a liquid crystal. a,**b**, Refractive index with birefringence (panel **a**) and absorption coefficient (panel **b**) of PCH5 for ordinary and extraordinary polarization at $T = 30$ °C. n_e, n_o represent the refractive indices and α_o and α_e the absorption coefficients for ordinary and extraordinary polarization. Birefringence Δn shown as a dashed line. Reprinted from ref. 85, Springer Nature Limited.

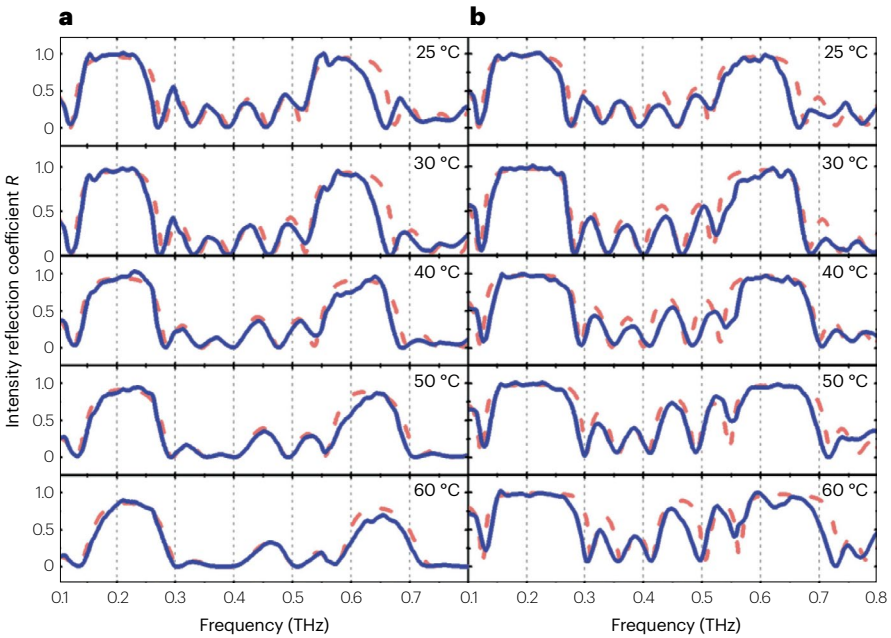

Fig. 6 | Intensity reflection spectrum of a one-dimensional photonic crystal composed of five layers. **a**, p-Polarized incident waves. **b**, s-Polarized incident waves. Solid blue and dashed red lines correspond to the measurement and simulations results, respectively. Adapted with permission from ref. 86, AIP.

these two conditions causes dehydration of the skin, which makes it more fragile and prone to produce wounds. Sensation becomes compromised and there is a poor immunological response in the area. This can result in infected ulcers, where the infection cannot be controlled and requires partial or total amputation of the limb. As skin hydration is affected by this condition, it is an area where terahertz waves can be used. In a recent proof-of-concept study, a small population of individuals with diabetes and individuals without diabetes were imaged with terahertz radiation to compare the foot skin water content of the two groups[88]. In a second study, 98 individuals without diabetes and 80 individuals with diabetes were imaged[83]. A statistically significant difference was found between feet hydration levels of patients with diabetes with existing feet complications and those without, as shown in Fig. 7a,b.

Reproducibility and data deposition

It is not yet general practice to make raw or processed terahertz TDS data publicly available. Therefore, there are no standards for deposition or commonly used repositories. As a result, it is difficult to assess the measurement reproducibility of terahertz TDS. In 2016, a study compared the refractive index and the absorption coefficient determined by terahertz TDS for a set of standard materials[89]. The measurements were performed by different laboratories worldwide, using different terahertz TDS systems. The study revealed variation between results, highlighting the need for a standardized measurement technique[89,90]. Frequency calibration and ensuring a linear detector response with respect to the terahertz electric field can be useful steps to ensure correct performance of the system[42,90]. Potential artefacts can be avoided and systematic errors can be reduced. Furthermore, correct modelling of how terahertz radiation interacts with the sample and correct data processing, for example phase retrieval[91], are essential to ensure correct results. Performing proper uncertainty analysis, including random and systematic uncertainty contributions[92,93], is useful when comparing results obtained in different laboratories employing different systems. Assessment of measurement repeatability can also be a valuable measure to compare results obtained with a single system[94,95]. Measurement repetition is especially useful when samples are investigated in reflection to determine the largest detectable absorption coefficient[52]. Simple measurement repetition can result in false identification of broad absorption features in the extracted absorption coefficient if the dynamic range of the spectrometer is unknowingly exceeded[52].

Limitations and optimizations

Terahertz TDS is a useful method to investigate samples in the terahertz range. Typical terahertz TDS systems cover a frequency range from roughly 100 GHz to several terahertz, which corresponds to a wavelength from 3 mm to about a hundred microns. Samples several millimetres in size can be investigated in the far field by focusing the terahertz beam onto the sample. When imaging a sample by raster scanning, the lateral resolution is limited by the focus size, which is dependent on the wavelength, and is in the order of hundreds of microns[5]. This limits the generation of microscopic images at terahertz frequencies. One unique approach is to form an emission image, based on the terahertz pulse emitted from an illuminated spot. The position of the laser is scanned across the material surface, producing an emission image. The image resolution is determined by the optical spot size, typically a few micrometres, rather than by the terahertz wavelength[96]. Alternatively, studying samples or sample features much smaller than the wavelength requires near-field techniques. A powerful approach is to combine a terahertz spectrometer with an atomic force microscope, an instrument that positions a sharp conductive tip close to the surface of a sample. When the terahertz beam is focused around the tip, the scattered radiation contains information about the dielectric properties of the sample region directly below the tip[97,98]. By scanning the tip across the sample surface, terahertz images can be formed with tip size-limited spatial resolution, comparable with the resolution of conventional atomic force microscope images[99]. This can

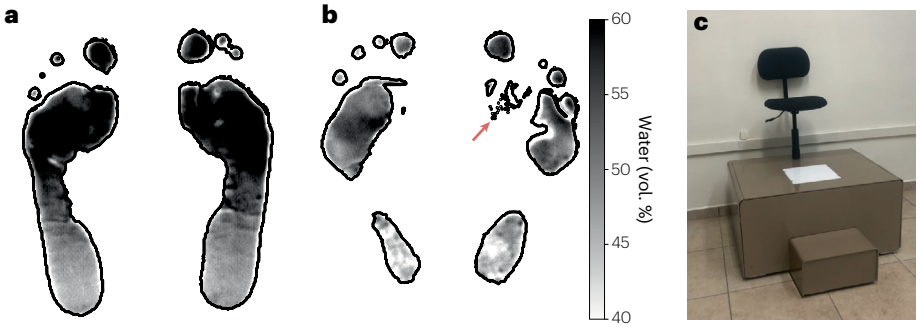

Fig. 7 | Terahertz imaging for the study of diabetic foot syndrome. a,**b**, Hydration images of a patient with diabetes with no complications (panel **a**) and a patient with diabetes with complications (panel **b**). An ulcer, covered by a patch (red arrow), is noticeable on the right metatarsal area of the patient with diabetes with complications, which, in turn, presents lower hydration along the foot sole compared with the patient with diabetes with no complications. **c**, Terahertz time-domain imaging set-up for feet. Adapted from ref. 83, Springer Nature Limited.

provide resolution below 100 nm, roughly 1,000 times smaller than the terahertz wavelength. There are several other techniques, including terahertz-assisted scanning tunnelling microscopy, which can provide atomic-scale spatial resolution in combination with sub-picosecond temporal resolution[100].

For tomographic investigations, depth resolution is an important property, alongside lateral resolution. The simplest experimental approach relies on directly identifying reflected terahertz pulses from interfaces that comprise the sample structure. The depth resolution is limited by the temporal width of the terahertz pulses. The resolution can be improved by using systems that cover a broader part of the terahertz spectrum, resulting in shorter pulses in the time domain. The depth resolution can be further improved with advanced deconvolution algorithms[101]. Appropriate modelling and fitting to measured frequency and time-domain data enabled the thickness of paint layers to be determined during drying with an error of a few micrometres[10]. As these measurements are conducted in the far field, the lateral resolution is wavelength limited. Imaging is performed by moving the sample with respect to the focus of the terahertz beam. For flat samples, this is achieved by mounting either the sample or the terahertz system — emitter, detector and terahertz optical components — on X–Y translation stages. For objects with three-dimensional curvature, there are additional strategies. One option is to incorporate a third stage for acquisition of multiple X–Y images at different sample angles to reconstruct three-dimensional axial tomographic images[102]. A second option is to use numerical reconstruction procedures, such as those used in seismic imaging, to form images from measurements at multiple receiver locations[103]. A third option is to use a robotic arm that can automatically adjust the transmitter angle in response to the local angle of the sample's top surface, based on optical image processing[9,10].

When samples are investigated in a laboratory environment, measurements can be performed under controlled conditions, for example under a nitrogen atmosphere, to avoid interaction of terahertz radiation with water vapour, which affects the measured terahertz signal (see Fig. 3). When larger objects are investigated, particularly if on-site investigation is needed or potential online industrial applications are considered, controlling the climate conditions is often not feasible. In such cases, numerical algorithms can be used to eliminate the effect of water vapour on the measured signal[104,105]. Observing absorption properties of gaseous water was one of the first terahertz spectroscopic measurements with a terahertz TDS system[106]. Investigating gases with terahertz TDS systems can be challenging due to the limited frequency resolution. The frequency resolution is fundamentally limited by the length of the recorded waveform in the time domain, which is limited by the length of the delay line. Often, this spectral resolution is not high enough to resolve the line shape of absorption lines in gaseous samples. Acquiring longer waveforms requires longer acquisition times. Alternative approaches can be used, such as asynchronous optical sampling[107] to replace the delay line and rapidly acquire long waveforms. However, actual improvements to the frequency resolution can be less than expected according to the Fourier theorem due to increased noise being sampled when longer waveforms are recorded[42,108].

Outlook

Terahertz TDS is still a method mostly used by specialists. Operation of the instrument and interpretation of measurement data often require trained personnel. Although these systems have been deployed in industrial settings[109], for more widespread adoption the operation of terahertz systems must become easier, so they can be operated by non-technically trained individuals. An example is the examination of cultural artefacts. In this context, it is important to examine objects for cavities and delamination before conservation[110]. These structures can lead to additional features in the reflected terahertz waveforms. For this type of application, a handheld device should be developed[111]. A handheld spectrometer should interpret the measured terahertz data with suitable software, possibly incorporating artificial intelligence. The operator would only be informed that the artefact is consolidated or that there may be a cavity at a measurement point. This vision may become a reality soon.

It can also be expected that more terahertz TDS systems will be manufactured in the future. This should have a favourable effect on their price. The technology should also become more compact. It is possible that fibre lasers may one day be replaced by semiconductor lasers, and the laser source, terahertz emitter and terahertz detector may be monolithically fabricated on a single chip. There are already efforts for photomixing terahertz systems in this direction.

This Primer aimed to give a clear introduction to terahertz TDS, an increasingly widespread measurement technique. The application fields are now so diverse that they cannot all be discussed in one article. Since it was first demonstrated in the late 1980s, measurement technology has developed considerably. In particular, the use of fibre lasers and fibre-coupled antenna modules has dramatically improved the flexibility and versatility. Today, terahertz systems can be used not only in research laboratories but also in industrial environments. However, they are not yet commonplace and remain unfamiliar to most. Although still not yet well known, the terahertz range is poised to have a significant impact on science and society.

Published online: 29 June 2023

References

1. Tonouchi, M. Cutting-edge terahertz technology. *Nat. Photonics* **1**, 97–105 (2007).
This work is one of the most comprehensive overviews on the state of the art about sources and detectors.
2. Leitenstorfer, A. et al. The 2023 terahertz science and technology roadmap. *J. Phys. D. Appl. Phys* **56**, 223001 (2023).
This work presents the broadest overview of the field to date.
3. Smith, P. R., Auston, D. H. & Nuss, M. C. Subpicosecond photoconducting dipole antennas. *IEEE J. Quantum Electron.* **24**, 255–260 (1988).
This pioneering publication introduces TDS.
4. Fattinger, C. & Grischkowsky, D. Terahertz beams. *Appl. Phys. Lett.* **54**, 490–492 (1989).
5. Hu, B. B. & Nuss, M. C. Imaging with terahertz waves. *Opt. Lett.* **20**, 1716–1718 (1995).
To our knowledge, this work is the first demonstration of time-domain imaging.
6. Chan, W. L., Deibel, J. & Mittleman, D. M. Imaging with terahertz radiation. *Rep. Prog. Phys.* **70**, 1325–1379 (2007).
7. Zhang, X. C. & Auston, D. H. Optoelectronic measurement of semiconductor surfaces and interfaces with femtosecond optics. *J. Appl. Phys.* **71**, 326–338 (1992).
8. Rudd, J. V., Zimdars, D. A. & Warmuth, M. W. in *Commercial and Biomedical Applications of Ultrafast Lasers II* Vol. 3934 (eds Neev, J. & Reed, M. K.) 27–35 (SPIE, 2000).
9. Stübling, E. et al. A THz tomography system for arbitrarily shaped samples. *J. Infrared Millim. Terahertz Waves* **38**, 1179–1182 (2017).
10. van Mechelen, J. L. M., Frank, A. & Maas, D. J. H. C. Thickness sensor for drying paints using THz spectroscopy. *Opt. Express* **29**, 7514–7525 (2021).
11. Grischkowsky, D., Keiding, S., van Exter, M. & Fattinger, C. H. Far-infrared time-domain spectroscopy with terahertz beams of dielectrics and semiconductors. *J. Opt. Soc. Am. B* **7**, 2006–2015 (1990).
12. Yasui, T., Saneyoshi, E. & Araki, T. Asynchronous optical sampling terahertz time-domain spectroscopy for ultrahigh spectral resolution and rapid data acquisition. *Appl. Phys. Lett.* **87**, 061101 (2005).
13. Janke, C., Först, M., Nagel, M., Kurz, H. & Bartels, A. Asynchronous optical sampling for high-speed characterization of integrated resonant terahertz sensors. *Opt. Lett.* **30**, 1405–1407 (2005).
14. Kim, Y. & Yee, D.-S. High-speed terahertz time-domain spectroscopy based on electronically controlled optical sampling. *Opt. Lett.* **35**, 3715–3717 (2010).
15. Dietz, R. J. B. et al. All fiber-coupled THz-TDS system with kHz measurement rate based on electronically controlled optical sampling. *Opt. Lett.* **39**, 6482–6485 (2014).
16. Wilk, R., Hochrein, T., Koch, M., Mei, M. & Holzwarth, R. OSCAT: novel technique for time-resolved experiments without moveable optical delay lines. *J. Infrared Millim. Terahertz Waves* **32**, 596–602 (2011).
17. Jördens, C. et al. Micro-mirrors for a multifocus terahertz imaging system. *J. Microw. Wirel. Technol.* **2**, 300–304 (2006).
18. Hunsche, S., Mittleman, D. M., Koch, M. & Nuss, M. C. New dimensions in T-ray imaging. *IEICE Trans. Electron.* **E81-C**, 269–276 (1998).
19. Beard, M. C., Turner, G. M. & Schmuttenmaer, C. A. Terahertz spectroscopy. *J. Phys. Chem. B* **106**, 7146–7159 (2002).
This work is probably the first widely used review in the field.
20. Kadlec, F., Kadlec, C., Kužel, P., Slavíček, P. & Jungwirth, P. Optical pump–terahertz probe spectroscopy of dyes in solutions: probing the dynamics of liquid solvent or solid precipitate? *J. Chem. Phys.* **120**, 912–917 (2004).
21. Richter, C. & Schmuttenmaer, C. A. Exciton-like trap states limit electron mobility in TiO_2 nanotubes. *Nat. Nanotechnol.* **5**, 769–772 (2010).
22. Pizzuto, A. et al. Nonlocal time-resolved terahertz spectroscopy in the near field. *ACS Photonics* **8**, 2904–2911 (2021).
23. Xiao, Z., Wang, J., Liu, X., Assaf, B. A. & Burghoff, D. Optical-pump terahertz-probe spectroscopy of the topological crystalline insulator $Pb_{1-x}Sn_xSe$ through the topological phase transition. *ACS Photonics* **9**, 765–771 (2022).
24. Schmuttenmaer, C. A. Exploring dynamics in the far-infrared with terahertz spectroscopy. *Chem. Rev.* **104**, 1759–1779 (2004).
25. Auston, D. H., Cheung, K. P. & Smith, P. R. Picosecond photoconducting Hertzian dipoles. *Appl. Phys. Lett.* **45**, 284–286 (1984).
26. Wilk, R. et al. in *Conf. Lasers and Electro-Optics (CLEO)* https://doi.org/10.1109/CLEO.2007.4452856 (Optica, 2007).
27. Dietz, R. J. B. et al. THz generation at 1.55 µm excitation: six-fold increase in THz conversion efficiency by separated photoconductive and trapping regions. *Opt. Express* **19**, 25911–25917 (2011).
28. Globisch, B. et al. Iron doped InGaAs: competitive THz emitters and detectors fabricated from the same photoconductor. *J. Appl. Phys.* **121**, 053102 (2017).
29. Jepsen, P. U., Jacobsen, R. H. & Keiding, S. R. Generation and detection of terahertz pulses from biased semiconductor antennas. *J. Opt. Soc. Am. B* **13**, 2424–2436 (1996).
30. Van Rudd, J., Johnson, J. L. & Mittleman, D. M. Cross-polarized angular emission patterns from lens-coupled terahertz antennas. *J. Opt. Soc. Am. B* **18**, 1524–1533 (2001).
31. Yang, K. H., Richards, P. L. & Shen, Y. R. Generation of far-infrared radiation by picosecond light pulses in LiNbO3. *Appl. Phys. Lett.* **19**, 320–323 (1971).
This work introduces terahertz generation by optical rectification.
32. Wu, Q. & Zhang, X. C. Free-space electro-optic sampling of terahertz beams. *Appl. Phys. Lett.* **67**, 3523–3525 (1995).
This work introduces electro-optic sampling.
33. Wu, Q. & Zhang, X. C. Free-space electro-optics sampling of mid-infrared pulses. *Appl. Phys. Lett.* **71**, 1285–1286 (1997).
34. Leitenstorfer, A., Hunsche, S., Shah, J., Nuss, M. C. & Knox, W. H. Detectors and sources for ultrabroadband electro-optic sampling: experiment and theory. *Appl. Phys. Lett.* **74**, 1516–1518 (1999).
35. Castro-Camus, E. et al. Photoconductive response correction for detectors of terahertz radiation. *J. Appl. Phys.* **104**, 053113 (2008).
36. Kužel, P., Němec, H., Kadlec, F. & Kadlec, C. Gouy shift correction for highly accurate refractive index retrieval in time-domain terahertz spectroscopy. *Opt. Express* **18**, 15338–15348 (2010).
37. Hintzsche, H. et al. Terahertz radiation at 0.380 THz and 2.520 THz does not lead to DNA damage in skin cells in vitro. *Radiat. Res.* **179**, 38–45 (2013).
38. Markelz, A. G. & Mittleman, D. M. Perspective on terahertz applications in bioscience and biotechnology. *ACS Photonics* **9**, 1117–1126 (2022).
This paper reviews biological applications.
39. Yeh, K.-L., Hoffmann, M. C., Hebling, J. & Nelson, K. A. Generation of 10 µJ ultrashort terahertz pulses by optical rectification. *Appl. Phys. Lett.* **90**, 171121 (2007).
40. Hough, C. M. et al. Disassembly of microtubules by intense terahertz pulses. *Biomed. Opt. Express* **12**, 5812–5828 (2021).
41. Vázquez-Cabo, J. et al. Windowing of THz time-domain spectroscopy signals: a study based on lactose. *Opt. Commun.* **366**, 386–396 (2016).
42. Withayachumnankul, W. & Naftaly, M. Fundamentals of measurement in terahertz time-domain spectroscopy. *J. Infrared Millim. Terahertz Waves* **35**, 610–637 (2014).
This work is an excellent reference on the processing of time-domain signals.
43. Naftaly, M. & Dudley, R. Methodologies for determining the dynamic ranges and signal-to-noise ratios of terahertz time-domain spectrometers. *Opt. Lett.* **34**, 1213–1215 (2009).
44. Duvillaret, L., Garet, F. & Coutaz, J.-L. Highly precise determination of optical constants and sample thickness in terahertz time-domain spectroscopy. *Appl. Opt.* **38**, 409–415 (1999).
This work is one of the first comprehensive methods for complex refractive index extraction with non-ideal samples.
45. Dorney, T. D., Baraniuk, R. G. & Mittleman, D. M. Material parameter estimation with terahertz time-domain spectroscopy. *J. Opt. Soc. Am. A Opt. Image Sci. Vis.* **18**, 1562–1571 (2001).
46. Pupeza, I., Wilk, R. & Koch, M. Highly accurate optical material parameter determination with THz time-domain spectroscopy. *Opt. Express* **15**, 4335–4350 (2007).
47. Huang, S. et al. Improved sample characterization in terahertz reflection imaging and spectroscopy. *Opt. Express* **17**, 3848–3854 (2009).
48. Pashkin, A., Kempa, M., Němec, H., Kadlec, F. & Kužel, P. Phase-sensitive time-domain terahertz reflection spectroscopy. *Rev. Sci. Instrum.* **74**, 4711–4717 (2003).
49. Jepsen, P. U., Møller, U. & Merbold, H. Investigation of aqueous alcohol and sugar solutions with reflection terahertz time-domain spectroscopy. *Opt. Express* **15**, 14717–14737 (2007).
50. Fan, S., Parrott, E. P. J., Ung, B. S. Y. & Pickwell-MacPherson, E. Calibration method to improve the accuracy of THz imaging and spectroscopy in reflection geometry. *Photonics Res.* **4**, A29–A35 (2016).
51. Thrane, L., Jacobsen, R. H., Uhd Jepsen, P. & Keiding, S. R. THz reflection spectroscopy of liquid water. *Chem. Phys. Lett.* **240**, 330–333 (1995).
52. Jepsen, P. U. & Fischer, B. M. Dynamic range in terahertz time-domain transmission and reflection spectroscopy. *Opt. Lett.* **30**, 29–31 (2005).
53. Hirori, H., Yamashita, K., Nagai, M. & Tanaka, K. Attenuated total reflection spectroscopy in time domain using terahertz coherent pulses. *Jpn J. Appl. Phys.* **43**, L1287 (2004).
54. Soltani, A. et al. Crystallization caught in the act with terahertz spectroscopy: non-classical pathway for L-(+)-tartaric acid. *Chem. Eur. J.* **23**, 14128–14132 (2017).
55. Chen, X. & Pickwell-MacPherson, E. An introduction to terahertz time-domain spectroscopic ellipsometry. *APL Photonics* **7**, 071101 (2022).
56. Astley, V., Reichel, K. S., Jones, J., Mendis, R. & Mittleman, D. M. Terahertz multichannel microfluidic sensor based on parallel-plate waveguide resonant cavities. *Appl. Phys. Lett.* **100**, 231108 (2012).
57. Laman, N., Harsha, S. S., Grischkowsky, D. & Melinger, J. S. High-resolution waveguide THz spectroscopy of biological molecules. *Biophys. J.* **94**, 1010–1020 (2008).
58. Jones, G. & Gordy, W. Submillimeter-wave spectra of HCl and HBr. *Phys. Rev.* **136**, A1229–A1232 (1964).
59. Messer, J. K., De Lucia, F. C. & Helminger, P. Submillimeter spectroscopy of the major isotopes of water. *J. Mol. Spectrosc.* **105**, 139–155 (1984).
60. Jepsen, P. U. & Clark, S. J. Precise ab-initio prediction of terahertz vibrational modes in crystalline systems. *Chem. Phys. Lett.* **442**, 275–280 (2007).
61. Siegrist, K. et al. High-resolution terahertz spectroscopy of crystalline trialanine: extreme sensitivity to β-sheet structure and cocrystallized water. *J. Am. Chem. Soc.* **128**, 5764–5775 (2006).
62. Ruggiero, M. T., Sibik, J., Orlando, R., Zeitler, J. A. & Korter, T. M. Measuring the elasticity of poly-L-proline helices with terahertz spectroscopy. *Angew. Chem. Int. Ed.* **55**, 6877–6881 (2016).
63. Łuczyńska, K., Drużbicki, K., Runka, T., Pałka, N. & Węsicki, J. Vibrational response of felodipine in the THz domain: optical and neutron spectroscopy versus plane-wave DFT modeling. *J. Infrared Millim. Terahertz Waves* **41**, 1301–1336 (2020).
64. Bawuah, P. & Zeitler, J. A. Advances in terahertz time-domain spectroscopy of pharmaceutical solids: a review. *TrAC. Trends Anal. Chem.* **139**, 116272 (2021).
65. Allis, D. G., Fedor, A. M., Korter, T. M., Bjarnason, J. E. & Brown, E. R. Assignment of the lowest-lying THz absorption signatures in biotin and lactose monohydrate by solid-state density functional theory. *Chem. Phys. Lett.* **440**, 203–209 (2007).

66. Ruggiero, M. T., Zhang, W., Bond, A. D., Mittleman, D. M. & Zeitler, J. A. Uncovering the connection between low-frequency dynamics and phase transformation phenomena in molecular solids. *Phys. Rev. Lett.* **120**, 196002 (2018).
67. Ruggiero, M. T. Invited review: modern methods for accurately simulating the terahertz spectra of solids. *J. Infrared Millim. Terahertz Waves* **41**, 491–528 (2020).
68. Zhang, W., Song, Z., Ruggiero, M. T. & Mittleman, D. M. Terahertz vibrational motions mediate gas uptake in organic clathrates. *Cryst. Growth Des.* **20**, 5638–5643 (2020).
69. Banks, P. A. et al. Thermoelasticity in organic semiconductors determined with terahertz spectroscopy and quantum quasi-harmonic simulations. *J. Mater. Chem. C. Mater* **8**, 10917–10925 (2020).
70. Schweicher, G. et al. Chasing the "Killer" phonon mode for the rational design of low-disorder, high-mobility molecular semiconductors. *Adv. Mater.* **31**, 1902407 (2019).
71. van Exter, M. & Grischkowsky, D. Optical and electronic properties of doped silicon from 0.1 to 2THz. *Appl. Phys. Lett.* **56**, 1694–1696 (1990).
72. Huggard, P. G. et al. Drude conductivity of highly doped GaAs at terahertz frequencies. *J. Appl. Phys.* **87**, 2382–2385 (2000).
73. Kaindl, R. A., Carnahan, M. A., Hägele, D., Lövenich, R. & Chemla, D. S. Ultrafast terahertz probes of transient conducting and insulating phases in an electron–hole gas. *Nature* **423**, 734–738 (2003).
74. Stein, M. et al. Dynamics of charge-transfer excitons in type-II semiconductor heterostructures. *Phys. Rev. B* **97**, 125306 (2018).
75. Bergren, M. R., Palomaki, P. K. B., Neale, N. R., Furtak, T. E. & Beard, M. C. Size-dependent exciton formation dynamics in colloidal silicon quantum dots. *ACS Nano* **10**, 2316–2323 (2016).
76. Bellissent-Funel, M.-C. et al. Water determines the structure and dynamics of proteins. *Chem. Rev.* **116**, 7673–7697 (2016).
77. Heugen, U. et al. Solute-induced retardation of water dynamics probed directly by terahertz spectroscopy. *Proc. Natl Acad. Sci. USA* **103**, 12301–12306 (2006).
78. Markelz, A. G. Terahertz dielectric sensitivity to biomolecular structure and function. *IEEE J. Sel. Top. Quantum Electron.* **14**, 180–190 (2008).
79. Niessen, K. A. et al. Protein and RNA dynamical fingerprinting. *Nat. Commun.* **10**, 1026 (2019).
80. Mittleman, D. M., Cunningham, J., Nuss, M. C. & Geva, M. Noncontact semiconductor wafer characterization with the terahertz Hall effect. *Appl. Phys. Lett.* **71**, 16–18 (1997).
81. Kanda, N., Konishi, K., Nemoto, N., Midorikawa, K. & Kuwata-Gonokami, M. Real-time broadband terahertz spectroscopic imaging by using a high-sensitivity terahertz camera. *Sci. Rep.* **7**, 42540 (2017).
82. Chen, A. et al. Non-contact terahertz spectroscopic measurement of the intraocular pressure through corneal hydration mapping. *Biomed. Opt. Express* **12**, 3438–3449 (2021).
83. Hernandez-Cardoso, G. G. et al. Terahertz imaging demonstrates its diagnostic potential and reveals a relationship between cutaneous dehydration and neuropathy for diabetic foot syndrome patients. *Sci. Rep.* **12**, 3110 (2022).
84. Wilk, R., Pupeza, I., Cernat, R. & Koch, M. Highly accurate THz time-domain spectroscopy of multilayer structures. *IEEE J. Sel. Top. Quantum Electron.* **14**, 392–398 (2008).
85. Vieweg, N., Shakfa, M. K., Scherger, B., Mikulics, M. & Koch, M. THz properties of nematic liquid crystals. *J. Infrared Millim. Terahertz Waves* **31**, 1312–1320 (2010).
86. Jansen, C., Wietzke, S., Astley, V., Mittleman, D. M. & Koch, M. Mechanically flexible polymeric compound one-dimensional photonic crystals for terahertz frequencies. *Appl. Phys. Lett.* **96**, 111108 (2010).
87. Lindley-Hatcher, H. et al. Real time THz imaging — opportunities and challenges for skin cancer detection. *Appl. Phys. Lett.* **118**, 230501 (2021).
88. Hernandez-Cardoso, G. G. et al. Terahertz imaging for early screening of diabetic foot syndrome: a proof of concept. *Sci. Rep.* **7**, 42124 (2017).
89. Naftaly, M. in *2016 41st Int. Conf. Infrared, Millimeter, and Terahertz Waves (IRMMW-THz)* https://doi.org/10.1109/IRMMW-THz.2016.7758763 (IEEE, 2016).
90. Naftaly, M., Clarke, R. G., Humphreys, D. A. & Ridler, N. M. Metrology state-of-the-art and challenges in broadband phase-sensitive terahertz measurements. *Proc. IEEE* **105**, 1151–1165 (2017).
91. Jepsen, P. U. Phase retrieval in terahertz time-domain measurements: a "how to" tutorial. *J. Infrared Millim. Terahertz Waves* https://doi.org/10.1007/s10762-019-00578-0 (2019).
92. Withayachumnankul, W., Fischer, B. M., Lin, H. & Abbott, D. Uncertainty in terahertz time-domain spectroscopy measurement. *J. Opt. Soc. Am. B* **25**, 1059–1072 (2008).
93. Yang, F. et al. Uncertainty in terahertz time-domain spectroscopy measurement of liquids. *J. Infrared Millim. Terahertz Waves* **38**, 229–247 (2017).
94. Méndez Aller, M., Abdul-Munaim, A., Watson, D. & Preu, S. Error sources and distinctness of materials parameters obtained by THz-time domain spectroscopy using an example of oxidized engine oil. *Sensors* **18**, 2087 (2018).
95. Ornik, J. et al. Repeatability of material parameter extraction of liquids from transmission terahertz time-domain measurements. *Opt. Express* **28**, 28178–28189 (2020).
96. Okada, K. et al. Scanning laser terahertz near-field reflection imaging system. *Appl. Phys. Express* **12**, 122005 (2019).
97. Knoll, B. & Keilmann, F. Near-field probing of vibrational absorption for chemical microscopy. *Nature* **399**, 134–137 (1999).
98. Zhan, H. et al. The metal-insulator transition in VO_2 studied using terahertz apertureless near-field microscopy. *Appl. Phys. Lett.* **91**, 162110 (2007).
99. Huber, A. J., Keilmann, F., Wittborn, J., Aizpurua, J. & Hillenbrand, R. Terahertz near-field nanoscopy of mobile carriers in single semiconductor nanodevices. *Nano Lett.* **8**, 3766–3770 (2008).
100. Cocker, T. L., Peller, D., Yu, P., Repp, J. & Huber, R. Tracking the ultrafast motion of a single molecule by femtosecond orbital imaging. *Nature* **539**, 263–267 (2016).
101. Dong, J., Wu, X., Locquet, A. & Citrin, D. S. Terahertz superresolution stratigraphic characterization of multilayered structures using sparse deconvolution. *IEEE Trans. Terahertz Sci. Technol.* **7**, 260–267 (2017).
102. Ferguson, B., Wang, S., Gray, D., Abbot, D. & Zhang, X.-C. T-ray computed tomography. *Opt. Lett.* **27**, 1312–1314 (2002).
103. Dorney, T. D. et al. Terahertz reflection imaging using Kirchhoff migration. *Opt. Lett.* **26**, 1513–1515 (2001).
104. Withayachumnankul, W., Fischer, B. M. & Abbott, D. Numerical removal of water vapour effects from terahertz time-domain spectroscopy measurements. *Proc. R. Soc. A Math. Phys. Eng. Sci.* **464**, 2435–2456 (2008).
105. Mikerov, M., Ornik, J. & Koch, M. Removing water vapor lines from THz-TDS data using neural networks. *IEEE Trans. Terahertz Sci. Technol.* **10**, 397–403 (2020).
106. van Exter, M., Fattinger, C. H. & Grischkowsky, D. Terahertz time-domain spectroscopy of water vapor. *Opt. Lett.* **14**, 1128–1130 (1989).
107. Klatt, G. et al. High-resolution terahertz spectrometer. *IEEE J. Sel. Top. Quantum Electron.* **17**, 159–168 (2011).
108. Mickan, S. P., Xu, J., Munch, J., Zhang, X.-C. & Abbott, D. The limit of spectral resolution in THz time-domain spectroscopy. *Photonics Des. Technol. Packag.* **5277**, 54–64 (2004).
109. Duling, I. & Zimdars, D. Terahertz imaging: revealing hidden defects. *Nat. Photonics* **3**, 630–632 (2009).
110. Lambert, F. E. M. et al. Layer separation mapping and consolidation evaluation of a fifteenth century panel painting using terahertz time-domain imaging. *Sci. Rep.* **12**, 21038 (2022).
111. Chen, X. et al. Terahertz (THz) biophotonics technology: instrumentation, techniques, and biomedical applications. *Chem. Phys. Rev.* **3**, 011311 (2022).

Author contributions

Introduction (M.K.); Experimentation (E.C.-C.); Results (D.M.M. and J.O.); Applications (M.K. and E.C.-C.); Reproducibility and data deposition (J.O. and D.M.M.); Limitations and optimizations (D.M.M., E.C.-C. and J.O.); Outlook (M.K.); Overview of the Primer (all authors).

Competing interests

The authors declare no competing interests.

Additional information

Supplementary information The online version contains supplementary material available at https://doi.org/10.1038/s43586-023-00232-z.

Peer review information *Nature Reviews Methods Primers* thanks Axel Zeitler, Young-Mi Bahk, Frederic Garet and Mona Jarrahi for their contribution to the peer review of this work.